First-principles study on ZnV$_2$O$_6$ and Zn$_2$V$_2$O$_7$

Sameie, H.; Sabbagh Alvani, A. A.; Naseri, N.; Du, S.; Rosei, F.

First-Principles Study on ZnV_2O_6 and $Zn_2V_2O_7$: Two New Photoanode Candidates for Photoelectrochemical Water Oxidation

H. Sameie [a,b], A.A. Sabbagh Alvani [b,*], N. Naseri [c], S. Du [d], F. Rosei [e]

[a] *Department of Polymer Engineering and Color Technology, Amirkabir University of Technology, Tehran 15875-4413, Iran*

[b] *Color & Polymer Research Center (CPRC), Amirkabir University of Technology, Tehran 15875-4413, Iran*

[c] *Department of Physics, Sharif University of Technology, Tehran 11155-9161, Iran*

[d] *School of Chemical Engineering, University of Birmingham, Edgbaston, Birmingham B15 2TT, UK*

[e] *INRS Centre for Energy, Materials and Telecommunications, Varennes, QC, J3X1P7, Canada*

[*] *Corresponding author:*

E-mail: sabbagh_alvani@aut.ac.ir

Tel: (+98-21) 66418600

Fax: (+98-21) 66418601

Abstract

First principles calculations based on density functional theory with generalized gradient approximation are performed to systematically investigate the structural, electronic and optical properties of two promising photoanodes, ZnV_2O_6 and $Zn_2V_2O_7$, for photocatalytic water splitting. After geometry optimization, the calculated structural parameters evince a satisfactory agreement with the experimental results indicating that the used method and conditions are suitable. The electronic structures demonstrate that both photocatalysts possess favorable band gaps (2.31 and 2.52 eV) and appropriate band edge positions for oxygen evolution reaction under solar radiation. We believe the relatively light effective masses at the valence band maximum and conduction band minimum result in enhanced photocatalytic activity owning to lower recombination probability of the photogenerated electrons and holes. Also, electronic density of states analysis displays that higher coordination number of vanadium in ZnV_2O_6 structure with respect to $Zn_2V_2O_7$ causes more delocalisation of bands due to lower V-V and O-O distances in conduction and valence bands, respectively. Meantime, optical properties such as dielectric function and optical absorption coefficient were computed to explore solar energy harvesting characteristics for solar water splitting application.

Keywords: *Oxygen evolution reaction, Ab-initio calculations, Band structure, Photocatalyst*

1. Introduction

Photocatalytic water splitting is a direct channel towards converting solar radiation to hydrogen and oxygen, whereby incident photons are consumed to drive the conversion of water into green fuel [1,3]. Theoretically, this process involves the electrons being excited from the valence band (VB) to the conduction band (CB) of the semiconductor photocatalyst by the absorbed photons forming the electron and hole pairs which can proceed the hydrogen evolution reaction (HER) H^+/H_2 ($2H^++2e^-\leftrightharpoons H_2$) and oxygen evolution reaction (OER) O_2/H_2O ($O_2+4H^++4e^-\leftrightharpoons 2H_2O$), respectively [4]. Development of an efficient photoelectrode for use in a water splitting photoelectrochemical cell (PEC) is extremely challenging due to some strict physical requirements including adequate band edge positions bracketing the water redox potentials, substantial overpotentials for oxidation of water to form oxygen or the reduction of protons to produce hydrogen and sufficiently small band gap to provide absorption overlap with the solar spectrum [5-7]. Furthermore, other practical parameters such as stability under the operation conditions and economic viability have led to continue further research to find the optimized photocatalysts [8,9].

Generally, modification of traditional photocatalysts [10,11] and development of a new photocatalyst or photocatalytic system [12,13] are two main aspects of the recent studies in the field of photosensitive materials for solar energy conversion. Therefore, many attempts have been made to explore new semiconductors for the half reaction of water splitting cells [14-16]. Among them, metal oxide semiconductors have attracted much attention, because of their relative stability against photocorrosion (photo-oxidative decomposition or dissolution), environmental affability and their low-cost fabrication [17-19]. Mixed metal vanadates have been widely investigated as photocatalyst due to narrow band gap, stable chemical property and excellent potential of photocatalytic activity [20-23]. However, to best knowledge of the authors, there are no reports so

far available to investigate transition metal vanadates ZnV_2O_6 and $Zn_2V_2O_7$ for solar water splitting applications. Nowadays, density functional theory (DFT) has known as an *ab-initio* technique to address a variety of fundamental properties to design new semiconductors for solar energy applications since some of these characteristics are quite difficult to be obtained experimentally. Thus, for a fundamental understanding we report the results of a comprehensive computational first-principles study based on DFT for ZnV_2O_6 and $Zn_2V_2O_7$ semiconductors to assess their photocatalytic potentials for solar water splitting systems.

2. Models and computational details

The first-principles calculations were carried out by means of DFT method based on total-energy plane-wave pseudopotential approach using the Cambridge Serial Total Energy Package (CASTEP) as implemented in Materials Studio [24]. The core electrons (Zn: [Ar] $3d^{10}$, V: [Ar] $3d^3$, O: [He]) were treated with the ultrasoft pseudopotential and the effects of exchange-correlation interactions of valence electrons (Zn: $4s^2$, V: $4s^2$, O: $2s^22p^4$) were evaluated by the revised Perdew-Burke-Ernzerhof (PBE) [25] for solid of generalized gradient approximation (GGA). Geometry optimization was done before single point energy calculation using GGA-PBE functionals with the dispersion correction according to Tkatchenko and Scheffler (TS) [26]. The numerical integrations were employed using the Monkhorst-Pack [27] grid with $3\times3\times2$ *k*-points in the Brillouin zone of the crystal to obtain the accurate density of the electronic states while the kinetic energy cutoff for wave function expansion was 340 eV and the self-consistent field (SCF) tolerance was set at 10^{-6} eV/atom. Furthermore, the convergence criterion for the maximal force between atoms was 0.01 eV/Å, the maximum displacement was 10^{-4} nm, and the stress was 0.02

Gpa, respectively. To verify the reliability of our results, we also performed a test calculation with different plane-wave cutoff energy and *k*-points.

3. Results and Discussion

At the first stage, the lattice constants and atomic positions of ZnV_2O_6 and $\alpha\text{-}Zn_2V_2O_7$ structures were optimized as a function of normal stress by minimizing the total energy. Both ZnV_2O_6 and $\alpha\text{-}Zn_2V_2O_7$ possess monoclinic crystal structure with space group *C2/m* and *C2/c*, respectively. The Zn^{2+} ions are octahedrally coordinated and the V^{5+} ions have an irregular octahedral coordination in ZnV_2O_6 structure. The VO_6 octahedra linked by edges can form infinite anionic layers and the ZnO_6 octahedra joined by opposite edges form infinite rows and link the anionic layers. On the other hand, $\alpha\text{-}Zn_2V_2O_7$ belongs to the family of pyro-compounds in which vanadium elements exhibit tetrahedral coordination with oxygen atoms forming V_2O_7 polyhedra [28,29]. The obtained structures of ZnV_2O_6 and $\alpha\text{-}Zn_2V_2O_7$ are illustrated in Fig. 1. Also, the calculated unit cell parameters for the optimized structures and their available experimental values [30-33] are compared in Table 1. The calculated equilibrium lattice constants are satisfactory consistent with the experimental data indicating the reliability of our DFT-based calculations. The existing discrepancy between the experimental values and the present theoretical values are usually caused by intrinsic approximations in the exchange-correlation functional and differences in the conditions of experimental (at room temperature) and theoretical (at 0 K) measurements [34].
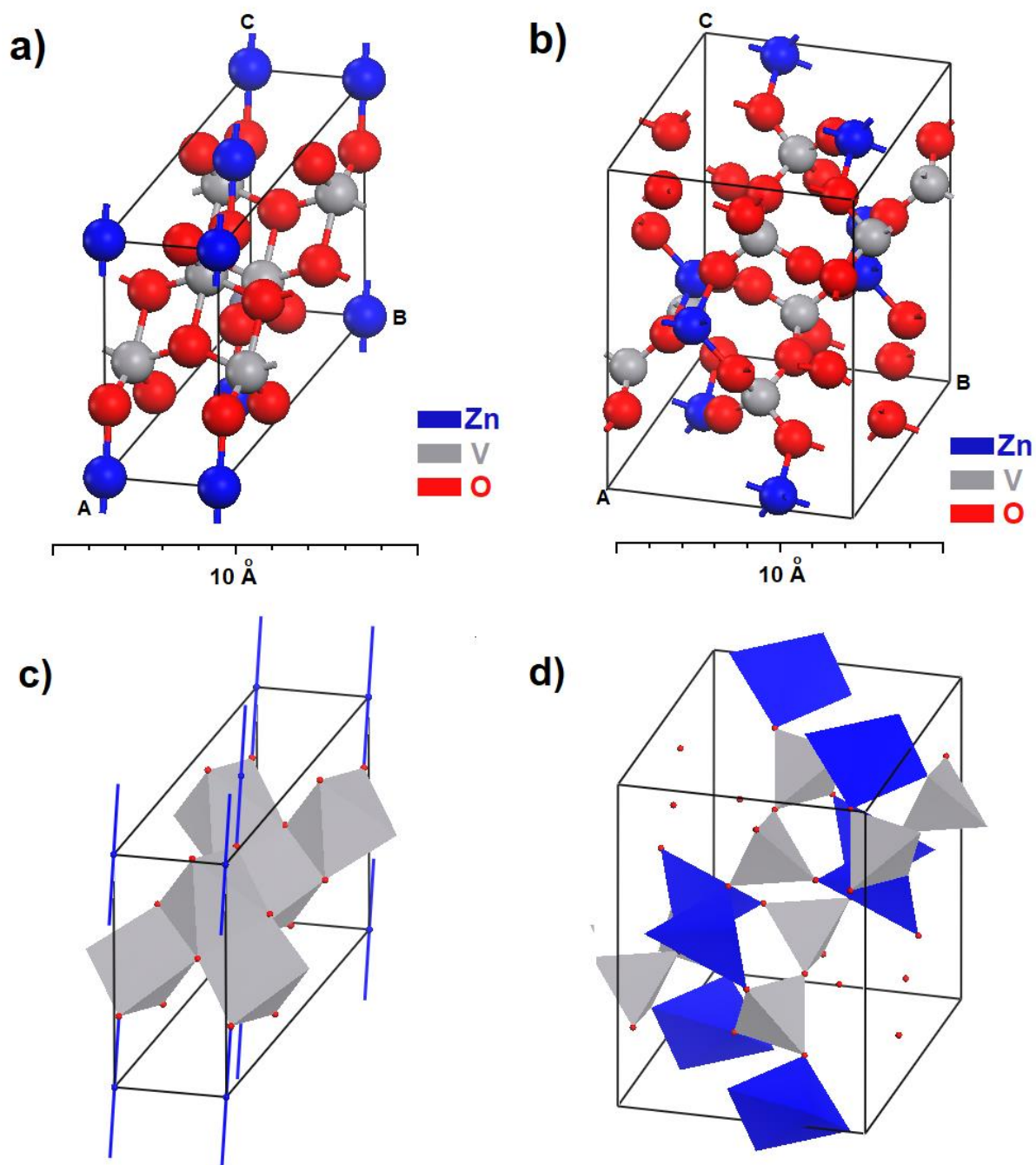
Fig. 1. DFT-optimized unit cells and the corresponding polyhedron structures of (a,c) ZnV$_2$O$_6$ and (b,d) α-Zn$_2$V$_2$O$_7$

Table 1. Calculated equilibrium lattice parameters compared with reported values

Compounds	Properties	Experimental Values	This Work	Average Deviation (%)	Ref.
ZnV_2O_6	a (Å)	9.245 / 9.223	9.026	3.847	30,31
	b (Å)	3.528 / 3.511	3.354		
	c (Å)	6.576 / 6.552	6.263		
α-$Zn_2V_2O_7$	a (Å)	7.43 / 7.429	7.129	3.413	32,33
	b (Å)	8.41 / 8.340	7.881		
	c (Å)	10.12 / 10.098	10.139		

The electronic properties can directly result in brilliant insights about photocatalysts which are candidates for solar water splitting applications. Electronic band-structure calculations of ZnV_2O_6 and $Zn_2V_2O_7$ were performed using the planewave based DFT and their computed band structures along the high symmetry directions of the Brillouin zone are depicted in **Fig. 2**. The calculated band gaps are 2.31 and 2.52 eV for ZnV_2O_6 and $Zn_2V_2O_7$, respectively which are within the range of band gap values reported for V_2O_5 (2.12 eV) and ZnO (3.3 eV) [35,36] and in agreement with the available few experimental reports [37,38]. The underestimated energy band gap values may be due to some DFT limitations because it does not consider the discontinuity in the exchange-

correlation potential [39]. The most effective approach to improve the conversion efficiency of solar water splitting is to reduce the band gap. Therefore, the semiconductors with visible light absorption (band gap in the range of 1.9 to 3 eV) are more demanding for this purpose because visible region corresponds to 43% of the direct sunlight at Earth's surface. Indeed, the band gap must be large enough to meet the thermodynamics and kinetics requirements for water splitting. Thermodynamically, a minimum energy would be required to overcome the standard Gibbs free energy change for water splitting reaction (1.23 eV) plus the thermodynamic losses (0.3-0.5 eV). Kinetically, an overpotential of 0.4-0.6 eV would be needed to enable a fast reaction. Hence, an ideal band gap can be considered in the range of 1.9-2.4 eV for solar water splitting [40,41]. Moreover, it is worth mentioning that smaller band gap leads to more vulnerability to photo-corrosion. Nevertheless, photocorrosion of semiconductors can be inhibited practically by addition of a sacrificial agent to the electrolyte. According to band structure profiles, ZnV_2O_6 and $Zn_2V_2O_7$ show quasi-direct and indirect band-gap natures, respectively. In the indirect band gap semiconductors, the valence band maximum (VBM) and conduction band minimum (CBM) are located at different k point promoting photocatalytic activity due to a longer traveling certain k space distance for excited carriers which decreases the recombination probability of the photogenerated electrons and holes. However, it should be noted that the absorption coefficient of indirect semiconductors are usually smaller than that of direct semiconductors because indirect transitions need absorption or emission of a phonon which is less likely to occur [42]. From **Fig 2** also it can be observed that the delocalisation of ZnV_2O_6 bands is greater than $Zn_2V_2O_7$ owning to higher coordination number of vanadium which results in lower V-V and O-O distances in conduction and valence bands, respectively. To further study the compositions of VBM and CBM for ZnV_2O_6 and $Zn_2V_2O_7$ semiconductors, the density of states (DOS) are computed. As presented

in **Fig. 3**, top of the valence band for both semiconductors is almost exclusively contributed by oxygen p orbitals with little d state contribution. Also, vanadium d states are main constituents of conduction band combined with a contribution of oxygen p and minor zinc s states. Eventually, valence band of ZnV_2O_6 seems broader than $Zn_2V_2O_7$ (spanning about 9 eV) as a consequence of more overlap between atomic wavefunctions which can facilitate hole transport through this semiconductor.
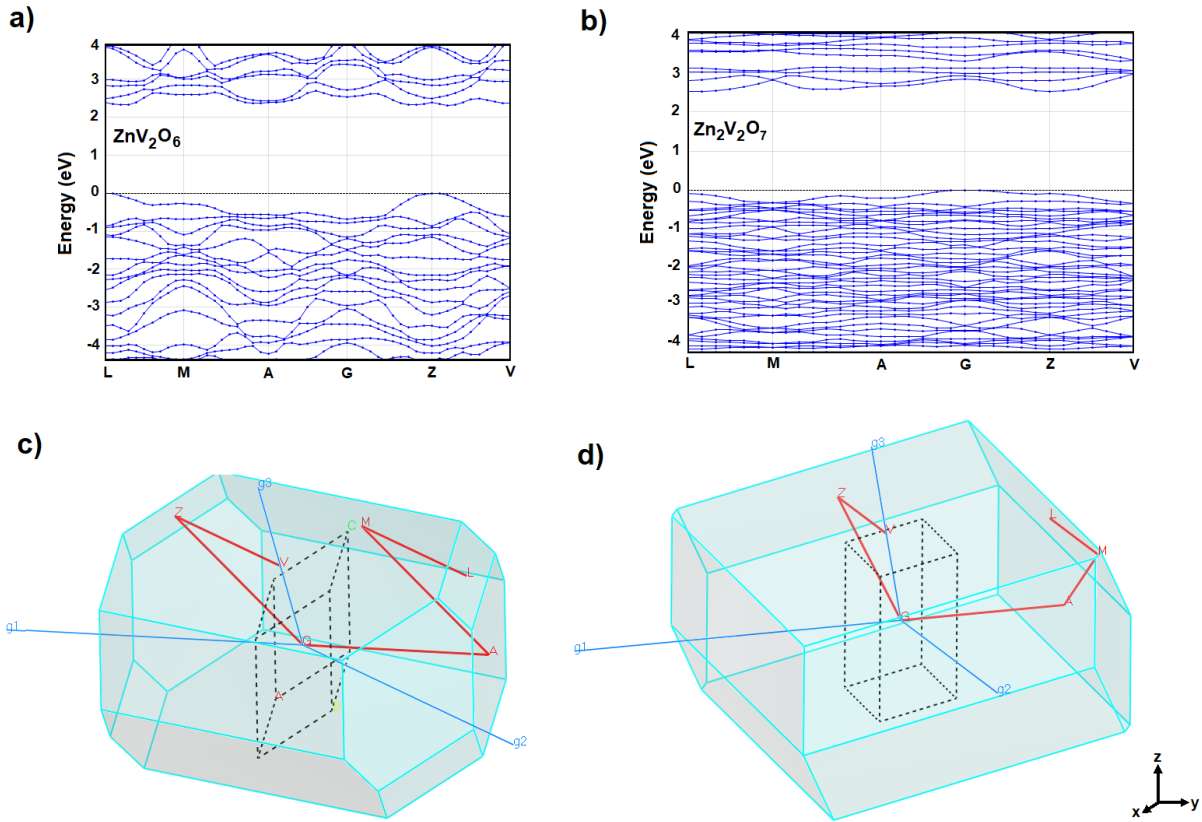
Fig. 2. Calculated GGA band structure and first Brillouin zones of (a,c) ZnV_2O_6 and (b,d) $Zn_2V_2O_7$ in the reciprocal lattice
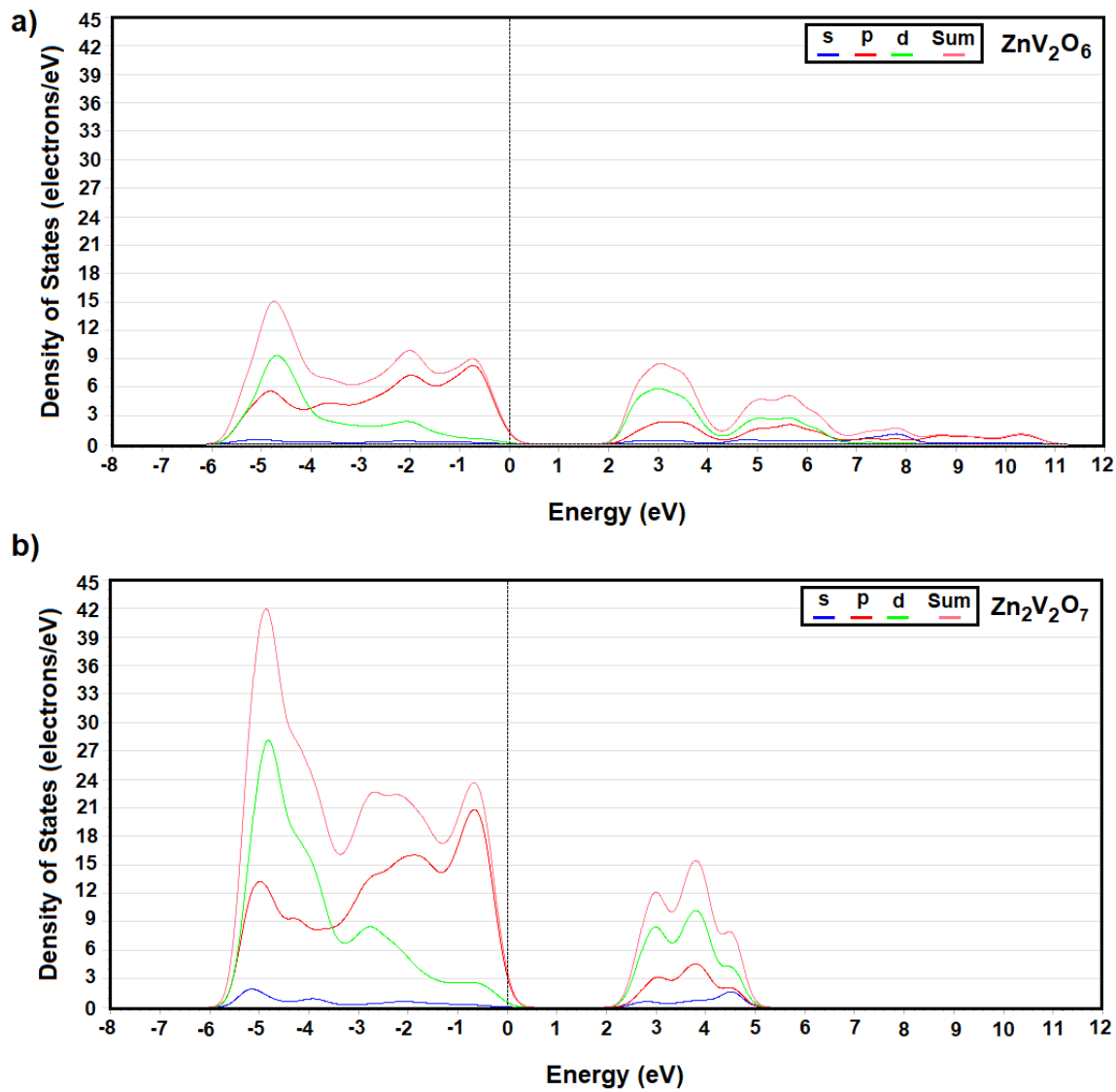
Fig. 3. Electronic densities of states of (a) ZnV_2O_6 and (b) $Zn_2V_2O_7$

Generally, the photocatalytic activity of a material is influenced by the amount of absorbed photons and the quantum efficiency as well. The former factor is identified with band gap, while the quantum efficiency is identified by separation efficiency of the photogenerated carriers. In addition to the adequate band gap to absorb photons in the visible region, there are other photophysical

requirements to design an appropriate photocatalyst for water-splitting reactions; (1) small effective masses of the charge carriers to achieve an acceptable mobility from bulk to surface; (2) suitable valence and conduction band edge positions based on water spitting limits to drive the photogenerated holes for oxidizing water at photoanode surface and similarly the photoexcited electrons for reducing H^+ at photocatode surface (3) high dielectric constant to reach an excellent exciton dissociation in the bulk into electron-hole pair. Thus, to further evaluate photocatalytic activity, we analyzed hese parameters for ZnV_2O_6 and $Zn_2V_2O_7$ semiconductors. The tensors of electron or hole effective masses at the band extremes are obtained from band dispersion by [43]

$$(m^*)_{ij} = \pm\hbar^2 \left(\frac{\partial^2 E_n(k)}{\partial k_i k_j}\right)^{-1} \quad (i,j = x,y,z) \tag{1}$$

where, $\hbar$ is the reduced Planck constant, i and j represent the reciprocal components and $E_n(k)$ is the k-space dispersion relation for the n-th band energy level. The effective masses of electrons and holes were calculated by parabola fitting of the dependence relationship of the energy to wave vector of ZnV_2O_6 and $Zn_2V_2O_7$ in three principal directions near the band extremes. Meanwhile, we computed the spherical average of electron and hole effective masses through [44]

$$\overline{m} = \frac{1}{4\pi} \int_0^{2\pi} \int_0^{\pi} m(\theta, \phi) \sin(\theta) \, d\theta \, d\phi \tag{2}$$

$$m(\theta, \phi) = \frac{1}{S_1 n_1^2 + S_2 n_2^2 + S_3 n_3^2} \tag{3}$$

here, θ and φ are azimuthal and polar angles in spherical coordinates, respectively and S_i represents the inverse of the effective mass of the i principal direction. The directional cosines are considered as $n_1=\sin(\theta)\cos(\varphi)$, $n_2=\sin(\theta)\sin(\varphi)$, and $n_3=\cos(\theta)$ in spherical coordinates. The values of the effective masses in three principal directions and the related spherical averages are summarized in

11

Table 2. In general, the effective masses of photogenerated electrons at the bottom of the CB and photogenerated holes on the top of VB for ZnV_2O_6 and $Zn_2V_2O_7$ are smaller than those of some studied semiconductor photocatalysts [45,47]. However, there are several strategies to further enhance charge carrier motility and diffusion length such as creating shallow-level states [48]. Furthermore, it seems the hole and electron are anisotropic in both structures which can favour the intralayer charge transport with respect to interlayer transport. The features of the orbitals that contribute to the CB and VB identify the localization and directionality of the charge distribution between lattice atoms usually resulting in the anisotropy of the charge carrier masses. The electronic band structure affects the charge carrier mobility, which is inversely proportional to the electron and hole effective masses. Therefore, for ZnV_2O_6, charge carrier masses reveal a relatively high mobility of the holes in the valence band compared to less mobile electrons in the conduction band. On the other hand, the results indicate a comparatively similar mobility of both charge carrier types in $Zn_2V_2O_7$ valence and conduction bands. The smaller average effective masses of electrons and holes for ZnV_2O_6 compared to $Zn_2V_2O_7$ is due to the more dispersive feature of conduction and valence bands, indicating the transfer of carriers to the reactive sites in ZnV_2O_6 would be rather easier in the photocatalytic process.

Table 2. Calculated effective masses of charge carriers in three principal directions and their spherical averages for ZnV₂O₆ and Zn₂V₂O₇

Compounds	electron				hole			
	[1 0 0]	[0 1 0]	[0 0 1]	average	[1 0 0]	[0 1 0]	[0 0 1]	average
ZnV_2O_6	0.74	3.68	1.18	1.41	1.93	0.99	4.87	2.03
$Zn_2V_2O_7$	1.69	18.62	0.82	2.48	1.34	9.51	1.18	2.27

The band edge positions are another significant metric for determining the capability of a photocatalyst to function in a photoelectrochemical cell producing hydrogen from sunlight. Regarding the redox potentials of water, the positions of electronic band edges of a semiconductor identify its ability to undergo photoinduced electron transfer to the adsorbed species on the surface. The conduction band potential (E_C) of the photo-cathode materials is thermodynamically required to be more negative than reduction potential of H^+/H_2 (0.0 V vs NHE) for HER, while the valence band potential (E_V) of the photo-anode materials needs to be more positive than oxidation potential of O_2/H_2O (1.23 V vs NHE) for OER. We speculated band edge positions for ZnV_2O_6 and $Zn_2V_2O_7$ photocatalysts according to a semi-empirical technique proposed by Butler and Ginley [49,50]. They demonstrated a relation between the electron affinities estimated through atomic Mulliken electronegativities and the measured flat band potential which is actually the Fermi energy of a material in water under applied bias at which no band bending occurs. According to this approach the band edge positions of a semiconductor at the point of zero charge can be expressed empirically by

$$E_V = \chi - E_e + 0.5E_g \qquad (4)$$

$$E_C = E_V - E_g \qquad (5)$$

where $E_e \approx 4.50$ eV is the scale factor relating the reference electrode redox level to the vacuum level and E_g is the band gap. The absolute electronegativity of a semiconductor, χ, defines as the geometric mean of the electronegativities of the constituent atoms obtained by

$$\chi \approx \left(\prod_{k=1}^{P} \chi_k \right)^{1/P} \qquad (6)$$

where P is the number of atoms in the crystal. The absolute electronegativities of ZnV_2O_6 and $Zn_2V_2O_7$ without considering the crystal structures and surface polarizations are 6.03 and 5.99 eV, respectively, which are computed from experimental electronegativity values (Zn = 4.45 eV, V = 3.6 eV and O = 7.54 eV) [51]. Therefore, relative band edge potentials of the semiconductors with respect to vacuum scale and normal hydrogen electrode (NHE) can be plotted in **Fig. 4**. For both semiconductors, the VB and CB edge positions are more positive than the oxidation potential of O_2/H_2O and the reduction potential of H^+/H_2, respectively. Therefore, they can be only used as photoanode materials for OER in solar water splitting cells. Also, the deep VB potentials cause that the surface collected holes have sufficient oxidation power at the surface of photoanodes without any need to add cocatalyst. Since the overpotential for OER can easily exceed 0.6 V for a metal oxide photoanode, co-catalysts such as RuO_2 are often used to enhance the reaction kinetics [52].
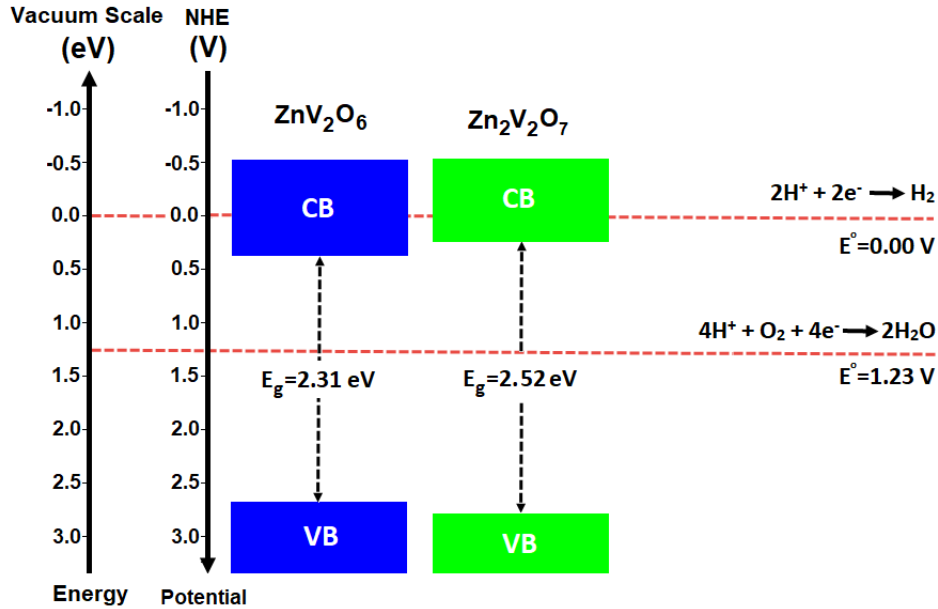
Fig. 4. Relative disposition of VB and CB potentials of ZnV_2O_6 and $Zn_2V_2O_7$ in comparison with redox potentials of water splitting

In order to investigate the solar energy harvesting property of ZnV_2O_6 and $Zn_2V_2O_7$ structures, the dielectric functions and absorption spectra were computed. Since the electric field vector of the incoming light polarizes the material, the optical properties can be determined from the transverse dielectric function $\varepsilon(q,\omega)$, where q is the momentum transfer in the photon-electron interaction and ω is the energy transfer. The complex dielectric function can be written in terms of the real $\varepsilon_1(\omega)$ and imaginary $\varepsilon_2(\omega)$ parts when the effect of momentum transfer from the initial state to the final state is not taken into consideration (Eq. 7). The $\varepsilon_2(\omega)$ describes the probability of the transitions between occupied to unoccupied states in the Brillouin zone and can be achieved through Eq. 8. The $\varepsilon_1(\omega)$ is subsequently derived from $\varepsilon_2(\omega)$ using the Kramer-Kronig dispersion transform (Eq. 9 and Eq. 10). Finally, the absorption coefficient $\alpha(\omega)$ is obtained by converting the complex dielectric function according to Eq. 11 [53,54].

$$\varepsilon(\omega) = \varepsilon_1(\omega) + i\varepsilon_2(\omega) \tag{7}$$

$$\varepsilon_2(\omega) = \frac{2\pi e^2}{\Omega \varepsilon_o} \sum_{k,V,C} \left| \langle \psi_k^C | \hat{u}.\vec{r} | \psi_k^V \rangle \right|^2 \delta(E_k^C - E_k^V - E) \tag{8}$$

$$\varepsilon_1(\omega) = 1 + \frac{2}{\pi} P \int_0^\infty \frac{\omega \prime \varepsilon_2(\omega\prime)d\omega\prime}{\omega\prime^2 - \omega^2} \tag{9}$$

$$P = \lim_{a\to 0} \int_{-\infty}^{\omega-a} \frac{\varepsilon(\omega\prime)}{\omega\prime - \omega} d\omega' + \lim_{a\to 0} \int_{\omega+a}^{+\infty} \frac{\varepsilon(\omega\prime)}{\omega\prime - \omega} d\omega' \tag{10}$$

$$\alpha(\omega) = \sqrt{2}\omega \left[\sqrt{\varepsilon_1^2(\omega) + \varepsilon_2^2(\omega)} - \varepsilon_1(\omega) \right]^{0.5} \tag{11}$$

In the mentioned equations, ω, Ω, e, $\vec{r}$, ε_o and E_i are the light frequency, the volume of the unit cell, the electronic charge, the electron's radius vector, the vacuum permittivity and the energy of electron in the i-th state, respectively. Also, $\hat{u}$ is the vector defining the polarization of the incident electric field, ψ_k^C and ψ_k^V are the conduction and valence band wave functions at k and P is the principal value of the integral, respectively. The imaginary and real parts of the dielectric function

of ZnV_2O_6 and $Zn_2V_2O_7$ are displayed in **Fig. 5**. The value of $\varepsilon_1(\omega)$ in zero energy which is known as the static dielectric constant is about 7 and 3.5 for ZnV_2O_6 and $Zn_2V_2O_7$, respectively. As a rule, higher static dielectric constant results in lower exciton binding energy of a photocatalyst and improves exciton dissociation into free charge carriers [55]. The negative values of $\varepsilon_1(\omega)$ in the energy range from 6.52 to 14.78 eV for ZnV_2O_6 and 6.04 to 10.92 eV for $Zn_2V_2O_7$ are ascribed to destruction of the electromagnetic wave, and zero values demonstrate that longitudinally polarized waves may happen. Since ZnV_2O_6 and $Zn_2V_2O_7$ are non-metal materials, the imaginary part of the complex dielectric function is attributed to the interband optical transitions between the different special *k* points at the first irreducible Brillouin zone. Therefore, the main peak in $\varepsilon_2(\omega)$ spectra can be attributed to the electronic transition from O *2p* (VB) to V *3d* (CB). As shown in **Fig. 6**, absorption plots depict wide and effective absorbency in both visible and ultraviolet light areas ensuring the suitable efficiency in solar water splitting.
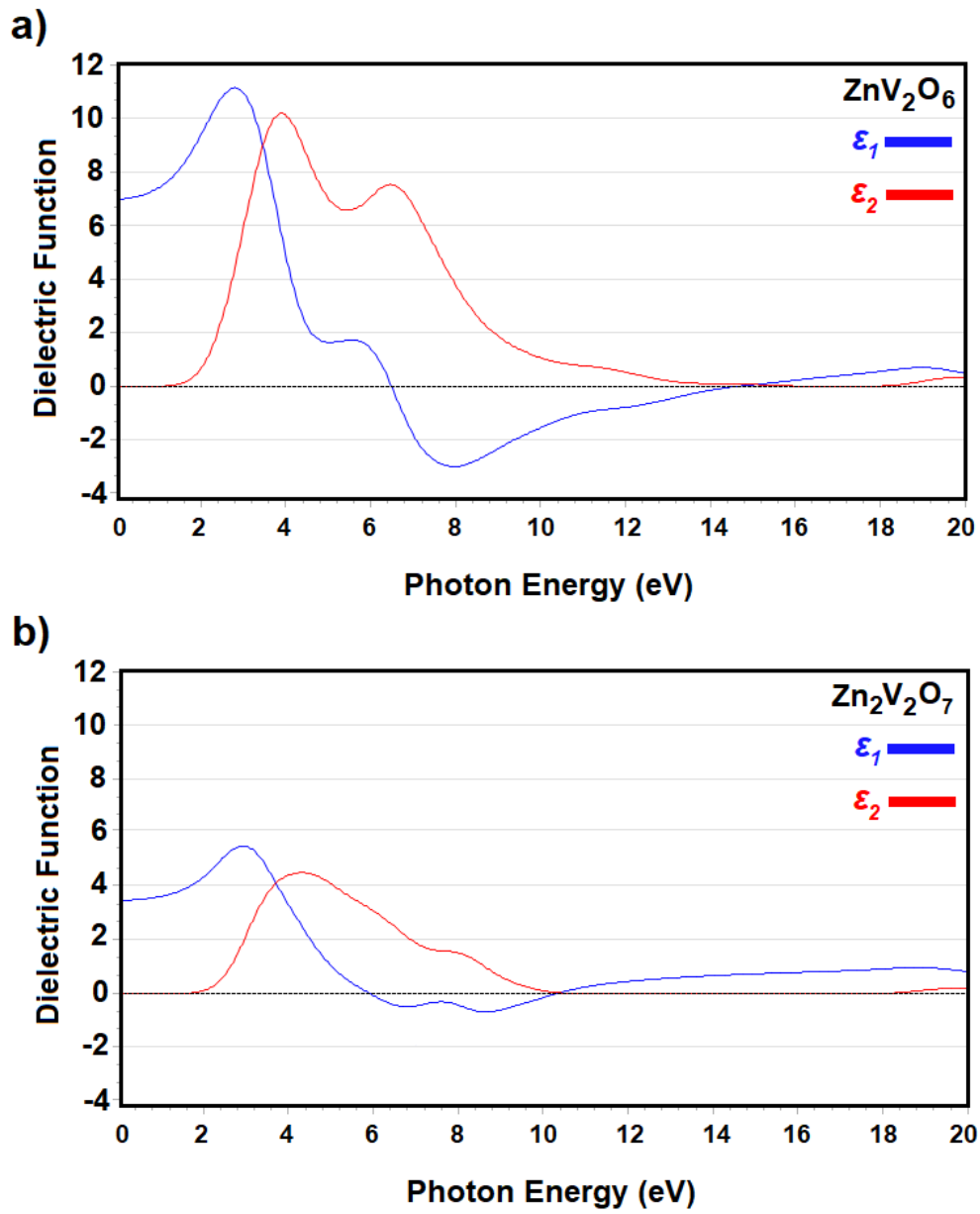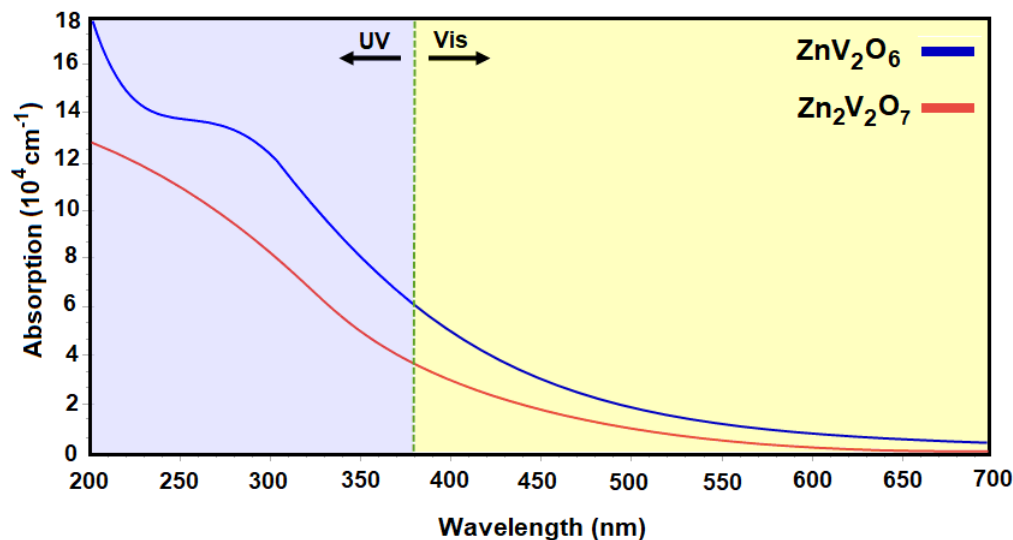
Fig. 5. The real part (ε_1) and the imaginary part (ε_2) of the dielectric functions of (a) ZnV_2O_6 and (b) $Zn_2V_2O_7$ as function of photon energy

Fig. 6. Optical absorption spectra of ZnV$_2$O$_6$ and Zn$_2$V$_2$O$_7$

Conclusion

In summary, essential fundamental properties of monoclinic ZnV$_2$O$_6$ and Zn$_2$V$_2$O$_7$ semiconductor materials for photocatalytic water splitting were theoretically investigated using first-principles computations on the basis of DFT within the PBE formalisms. The equilibrium lattice parameters, the band gaps, the dielectric constants, the optical absorption coefficients and the band edge energy positions of these compounds were evaluated and discussed in detail. Both ZnV$_2$O$_6$ and Zn$_2$V$_2$O$_7$ semiconductors with calculated band gaps of 2.31 and 2.52 eV, respectively met all photo-physical requirements for water oxidation without the need to use cocatalyst owning to deep VB edge energy positions which are sufficiently more positive than the oxidation potential of O$_2$/H$_2$O. In additions, the satisfactory optical characteristics and charge carrier transport properties predicted for ZnV$_2$O$_6$ and Zn$_2$V$_2$O$_7$ compounds will certainly offer a grand opportunity for these photocatalysts to be properly synthesized and tested for photocatalytic oxygen generation from water splitting.

References

[1] A. Fujishima, K. Honda, Electrochemical photolysis of water at a semiconductor electrode, Nature 238 (1972) 37-38.

[2] H. Pan, Principles on design and fabrication of nanomaterials as photocatalysts for water splitting, Renew. Sust. Energ. Rev. 57 (2016) 584-601.

[3] S. Moniz, S. Shevlin, A.D. Martin, Z. Guo, J. Tang, Visible-light driven heterojunction photocatalysts for water splitting - a critical review, Energy Environ. Sci. 8 (2015) 731-759.

[4] M.G. Walter, E.L. Warren, J.R. McKone, S.W. Boettcher, Q. Mi, E.A. Santori, N.S. Lewis, Solar water splitting cells, Chem. Rev. 110 (2010) 6446-6473.

[5] R.M. Navarro, F. del Valle, J.A. Villoria de la Mano, M.C. Alvarez-Galvan, J.L.G. Fierro, Photocatalytic water splitting under visible light: concept and catalysts development, Adv. Chem. Engineer. 36 (2009) 111-143.

[6] J. Liu, Y. Liu, N. Liu, Y. Han, X. Zhang, H. Huang, Y. Lifshitz, S.T. Lee, J. Zhong, Z. Kang, Metal-free efficient photocatalyst for stable visible water splitting via a two-electron pathway, Science 347 (2015) 970-974.

[7] H.J. Lewerenz, P. Laurence, Photoelectrochemical Water Splitting: Materials, Processes and Architectures, RSC Publishing, Cambridge, 2013.

[8] Z. Zhu, C.T. Kao, B.H. Tang, W.C. Chang, R.J. Wu, Efficient hydrogen production by photocatalytic water-splitting using Pt-doped TiO_2 hollow spheres under visible light, Ceram. Int. 42 (2016) 6749-6754.

[9] S.Y. Tee, K.Y. Win, W.S. Teo, L.D. Koh, S. Liu, C.P. Teng, M.Y. Han, Recent progress in energy-driven water splitting, Adv. Sci. 4 (2017) 1600337-1600360.

[10] T.W. Kim, Y. Ping, G.A. Galli, K.S. Choi, Simultaneous enhancements in photon absorption and charge transport of bismuth vanadate photoanodes for solar water splitting, Nat. Commun. 6 (2015) 8769-8778.

[11] T. W. Kim, Y. Ping, G.A. Galli, K.S. Choi, S. Filice, G. Compagnini, R. Fiorenza, S. Scire, L. D'Urso, M.E. Fragala, P. Russo, E. Fazio, S. Scalese, Laser processing of TiO_2 colloids for an enhanced photocatalytic water splitting activity, J. Colloid Interface Sci. 489 (2017) 131-137.

[12] H. Li, H. Hu, C. Bao, F. Guo, X. Zhang, X. Liu, J. Hua, J. Tan, A. Wang, H. Zhou, B. Yang, Y. Qu, X. Liu, Forming heterojunction: an effective strategy to enhance the photocatalytic efficiency of a new metal-free organic photocatalyst for water splitting, Sci. Rep. 6 (2016) 2932-2941.

[13] M. Higashi, K. Domen, R. Abe, Fabrication of an efficient $batao_2n$ photoanode harvesting a wide range of visible light for water splitting, J. Am. Chem. Soc. 135 (2013) 10238-10241.

[14] J. Luan, J. Chen, Photocatalytic Water splitting for hydrogen production with novel $y2msbo7$ (m = ga, in, gd) under visible light irradiation, Materials 5 (2012) 2423-2438.

[15] Z.Y. Zhao, Q.L. Liu, W.W. Dai, Structural, electronic and optical properties of $BiOX_{1-x}Y_x$ (X, Y = F, Cl, Br, and I) solid solutions from DFT calculations, Sci. Rep. 6 (2016) 31449-31460.

[16] P. Dhanasekaran, N.M. Gupta, Factors affecting the production of H_2 by water splitting over a novel visible-light-driven photocatalyst $GaFeO_3$, Int. J. Hydrogen Energy 37 (2012) 4897-4907.

[17] Y. Zhang, Z. Zhou, C. Chen, Y. Che, H. Ji, W. Ma, J. Zhang, D. Song, J. Zhao, Gradient $FeO_x(PO_4)_y$ layer on hematite photoanodes: novel structure for efficient light-driven water oxidation, ACS Appl. Mater. Interfaces 6 (2014) 12844-12851.

[18] H. Ahmad, S.K. Kamarudin, L.J. Minggu, M. Kassim, Hydrogen from photo-catalytic water splitting process: A review, Renew. Sust. Energ. Rev. 43 (2015) 599-610.

[19] S.K. Biswas, J.O. Baeg, Enhanced photoactivity of visible light responsive W incorporated $FeVO_4$ photoanode for solar water splitting, Int. J. Hydrogen Energy 38 (2013) 14451-14457.

[20] H.X. Dang, A.J.E. Rettie, C.B. Mullins, Visible-light-active NiV_2O_6 films for photoelectrochemical water oxidation, J. Phys. Chem. C 119 (2015) 14524-14531.

[21] Q. Yan, G. Li, P.F. Newhouse, J. Yu, K.A. Persson, J.M. Gregoire, J.B. Neaton, $Mn_2V_2O_7$: An earth abundant light absorber for solar water splitting, Adv. Energy Mater. 5 (2015) 1401840-1401845

[22] H. Mandal, S. Shyamal, P. Hajra, A. Bera, D. Sariket, S. Kundu, C. Bhattacharya, Development of ternary iron vanadium oxide semiconductors for applications in photoelectrochemical water oxidation, RSC Adv. 6 (2016) 4992-4999.

[23] W. Guo, W.D. Chemelewski, O. Mabayoje, P. Xiao, Y. Zhang, C.B Mullins, Synthesis and characterization of CuV_2O_6 and $Cu_2V_2O_7$: Two photoanode candidates for photoelectrochemical water oxidation, J. Phys. Chem. C 119 (2015) 27220-27227.

[24] S.J. Clark, M.D. Segall, C.J. Pickard, P.J. Hasnip, Probert, K. Refson, Payne, M.C. Payne, First principles methods using CASTEP, Cryst. Mater. 220 (2005) 567-570.

[25] J.P. Perdew, K. Burke, M. Ernzerhof, Generalized gradient approximation made simple, Phys. Rev. Lett. 77 (1996) 3865-3868.

[26] A. Tkatchenko, M. Scheffler, Accurate molecular van der Waals interactions from ground-state electron density and free-atom reference data, Phys. Rev. Lett. 102 (2009) 73005.

[27] J.D. Pack, H.J. Monkhorst, Special points for Brillouin-zone integrations - a reply, Phys. Rev. B 16 (1977) 1748-1749.

[28] G.D. Andreetti, G. Calestani, A. Montenero, M. Bettinelli, Refinement of the crystal structure of ZnV_2O_6, Z. Kristallogr. 168 (1984) 53-58.

[29] R. Gopal, C. Calvo, Crystal Structure of α-$Zn_2V_2O_7$, Can. J. Chem. 51 (1973) 1004-1009.

[30] F.K. Butt, F. Idrees, M. Tahir, C. Cao, R. Hussain, R. Ahmed, B. Ul-Haq, Fabrication of ZnV_2O_6 nanostructures: Their energy storage and PL properties, Mater. Lett. 155 (2015) 15-17.

[31] H. Liu, D. Tang, Synthesis of ZnV_2O_6 powder and its cathodic performance for lithium secondary battery, Mater. Chem. Phys. 114 (2009) 656-659.

[32] F.K. Butt, C. Cao, F. Idrees, M. Tahir, R. Hussain, R. Ahmed, W.S. Khan, Novel $Zn_2V_2O_7$ hierarchical nanostructures: Optical and hydrogen storage properties, Int. J. Hydrogen Energy 40 (2015) 9359-9364.

[33] N. Venugopal, W.S. Kim, New α-$Zn_2V_2O_7$/carbon nanotube nanocomposite for supercapacitors, Korean J. Chem. Eng. 32 (2015) 1918-1923.

[34] E. Zahedi, M. Hojamberdiev, M.F. Bekheet, Electronic, optical and photocatalytic properties of three-layer perovskite Dion-Jacobson phase $CsBa_2M_3O_{10}$ (M = Ta, Nb): A DFT study, RSC Adv. 5 (2015) 88725-88735.

[35] S. Beke, A review of the growth of V_2O_5 films from 1885 to 2010, Thin Solid Films 519 (2011) 1761-1771.

[36] N. Ashkenov, B.N. Maenkum, C. Bundenn, V. Riede, M. Lorenz, D. Spemann, E. M. Kaideshev, A. Basic, M. Schubert, M. Grundmann, G. Wagner, H. Neumann, V. Darakchieva, H. Arwin, B. Monemar, Infreared dielectric functions and phonon modes of high-quality ZnO films, J. Appl. Phys. 93 (2003) 126-133.

[37] S.M. Ji, S.H. Choi, J.S. Jang, E.S. Kim, J.S. Lee, Band gap tailored $Zn(Nb_{1-x}V_x)_2O_6$ solid solutions as visible light photocatalysts, J. Phys. Chem. C 113 (2009) 17824-17830.

[38] Y.A. Gonzalez-Rivera, A.N. Meza-Rocha, L. Aquino-Meneses, S. Jimenez-Sandoval, E. Rubio-Rosas, U. Caldino, E. Alvarez, O. Zelaya-Angel, M. Toledo-Solano, R. Lozada-Morales, Photoluminescent and electrical properties of novel Nd^{3+} doped ZnV_2O_6 and $Zn_2V_2O_7$, Ceram. Int. 42 (2016) 8425-8430.

[39] E. Kraisler, L. Kronik, Fundamental gaps with approximate density functionals: The derivative discontinuity revealed from ensemble considerations, J. Chem. Phys. 140 (2014) 18A540-18A549.

[40] A.B. Murphy, P.R.F. Barnes, L.K. Randeniya, I.C. Plumb, I.E. Grey, M.D. Horne, Efficiency of solar water splitting using semiconductor electrodes, Int. J. Hydrogen Energy 31 (2006) 1999-2017.

[41] J.R. Bolton, A.F. Haught, R.T. Ross, J.S. Connolly (Ed.), Photochemical Energy Storage: An Analysis of Limits, In Photochemical Conversion and Storage of Solar Energy, Academic Press, New York, 1981.

[42] T. Tong, X. Wei, G. Zhu, Y. Huang, First-principles studies on facet-dependent photocatalytic properties of BiOI {001} surface, J. Mater. Sci. 52 (2017) 5686-5695.

[43] C. Kittle, Introduction to Solid State Physics, eighth ed., John Wiley & Sons, Inc., New York, 2005.

[44] J. Feng, B.J. Xiao, Effective masses and electronic and optical properties of nontoxic $MASnX_3$ (X = Cl, Br, and I) perovskite structures as solar cell absorber: A theoretical study using HSE06, Phys. Chem. C 118 (2014) 19655-19660.

23

[45] T. Luttrell, S. Halpegamage, J. Tao, A. Kramer, E. Sutter, M. Batzill, Why is anatase a better photocatalyst than rutile? Model studies on epitaxial TiO_2 films, Sci. Rep. 4 (2014) 4043-4050.

[46] X. Ma, Y. Dai, M. Guo, B. Huang, The role of effective mass of carrier in the photocatalytic behavior of silver halide-based Ag@AgX (X=Cl, Br, I): A theoretical study, ChemPhysChem13 (2012) 2304-2309.

[47] E. Zahedi, B. Xiao, M. Shayestefar, First-principles investigations of the structure, electronic, and optical properties of mullite-type orthorhombic $Bi_2M_4O_9$ (M = Al^{3+}, Ga^{3+}), Inorg. Chem. 55 (2016) 4824-4835.

[48] P. Salvador, Analysis of the physical properties of TiO_2:Be electrodes in the photoassisted oxidation of water, Solar Energy Mater. 6 (1982) 241-250.

[49] M.A. Butler, D.S. Ginley, Prediction of flatband potentials at semiconductor-electrolyte interface from atomic electronegativitics. J. Electrochem. Soc. 125 (1978) 228-232.

[50] J. Liu, S. Chen, Q. Liu, Y. Zhu, Y. Lu, Density functional theory study on electronic and photocatalytic properties of orthorhombic $AgInS_2$, Comput. Mater. Sci. 91 (2014) 159-164.

[51] R.G. Pearson, Absolute electronegativity and hardness: application to inorganic chemistry, Inorg. Chem. 27 (1988) 734-740.

[52] S. Licht, B. Wang, S. Mukerji, T. Soga, M. Umeno, H. Tributsch, Efficient solar water splitting, exemplified by RuO_2-catalyzed AlGaAs/Si photoelectrolysis. J. Phys. Chem. B 104 (2000) 8920-8924.

[53] R. Paschotta, Encyclopedia of Laser Physics and Technology, first ed., Wiley-VCH, New York, 2008.

24

[54] P. Li, W. Fan, Y. Li, H. Sun, X. Cheng, X. Zhao, M. Jiang, First-principles study of the electronic, optical properties and lattice dynamics of tantalum oxynitride, Inorg. Chem. 49 (2010) 6917-6924.

[55] S.Y. Leblebici, T.L. Chen, P.O. Velasco, W. Yang, B. Ma, Reducing exciton binding energy by increasing thin film permittivity: an effective approach to enhance exciton separation efficiency in organic solar cells, ACS Appl. Mater. Interfaces 5 (2013) 10105-10110.